JOURNAL OF GEOPHYSICAL RESEARCH, VOL. 90, NO. B11, PAGES 9411–9421, SEPTEMBER 30, 1985

The LAGEOS Constraint on Deep Mantle Viscosity: Results From a New Normal Mode Method for the Inversion of Viscoelastic Relaxation Spectra

W. R. PELTIER

Department of Physics, University of Toronto, Canada

The recently observed acceleration in the node of the orbit of the LAGEOS satellite has previously been shown to provide a good constraint on the viscosity of the earth's mantle beneath the 670-km seismic discontinuity. This paper explores the extent to which the previously inferred lower mantle viscosity may be traded off against variations of other properties of the radial viscoelastic structure. We show explicitly that the nontidal acceleration of rotation inferred from the LAGEOS data, and predicted as a consequence of the earth's response to the last deglaciation event of the current ice age, is relatively insensitive both to variations of lithospheric thickness and to the presence or absence of plausible chemical heterogeneity across the 670-km interface. It therefore provides a high-quality constraint on the viscosity of the deep mantle. With the upper mantle viscosity fixed at the nominal value of 10^{21} Pa s, the bounds on lower mantle viscosity ν_{LM} are such that 2×10^{21} Pa s $\leq \nu_{LM} \leq \sim 6 \times 10^{21}$ Pa s even when allowance is made for the presence of a viscous boundary layer at the base of the upper mantle such as would exist if the mantle convective circulation were layered.

1. INTRODUCTION

Analysis of $5\frac{1}{2}$ years of orbital data for the LAGEOS satellite, reported by *Yoder et al.* [1983], established rather convincingly that there exists a residual acceleration in the node of the orbit in the amount -14.7 ± 1.3 m arc s yr^{-2}. This acceleration is predominantly attributable to a secular decrease of the degree 2 component of the earth's gravitational potential field, J_2, at the rate $\dot{J}_2 = (-3.5 \pm 0.3) \times 10^{-11}$ yr^{-1}. It is furthermore in accord with the nontidal acceleration of rotation previously inferred through analyses of ancient eclipse data (for example, see *Peltier* [1982] and references cited therein). Using a deglaciation history for the earth following the last glacial maximum 18,000 yr B.P. tabulated by *Wu and Peltier* [1983], Yoder et al. employed a very simple theory of the rotational response of the earth to deglaciation to show that the observed $\dot{J}_2$ might be explained as a response of the earth to ice sheet disintegration. This analysis was confirmed and refined by *Peltier and Wu* [1983], *Peltier* [1983], and *Wu and Peltier* [1984], who demonstrated that the datum could be inverted to obtain a strong constraint on the viscosity of the deep mantle if the LAGEOS observation were considered in conjunction with other isostatic adjustment data, such as relative sea level and free air gravity observations [e.g., *Peltier*, 1982]. That an observation of $\dot{J}_2$ might provide such information had been predicted by *Peltier* [1982]. With these additional constraints the LAGEOS observation was shown to require a lower mantle viscosity ν_{LM} such that 2.7×10^{21} Pa s $\leq \nu_{LM} \leq 4.4 \times 10^{21}$ Pa s (note that 1 Pa s = 10 poise). This is the tightest bound on this important parameter that has been established. It is therefore interesting to enquire as to whether tradeoffs between ν_{LM} and other characteristics of the radial viscoelastic structure might exist which could significantly degrade these bounds. Although I will employ the Yoder et al. number for $\dot{J}_2$ in what follows, it is important to be aware that an independent analysis of the LAGEOS orbit by *Rubincam* [1984] has recently led to a somewhat lower value of $\dot{J}_2 = (-2.6 \pm 0.6) \times 10^{-11}$ yr^{-1} with a somewhat larger measurement error. *Alexander* [1983] has furthermore investigated the contributions of the zonal coefficients J_4 and J_6 to the acceleration of the node of the orbit and shown their effects to be small in relation to that of J_2 but perhaps not completely negligible in relation to those of the geophysical parameters upon which I will focus exclusively below. The interpretations which I provide must be considered in the light of these additional qualifications of which I have not attempted to take explicit account.

In this paper I will consider comparisons between predicted and observed $\dot{J}_2$ in the context of particularly simple parameterizations of the radial viscoelastic structure. The models all have reasonable earth mass and moment of inertia, an inviscid core of the correct radius and density, and a mantle viscoelastic structure which is characterized by four main parameters. These four parameters are the upper and lower mantle densities ρ_{UM}, ρ_{LM} and the upper and lower mantle viscosities ν_{UM}, ν_{LM}. The boundary between the upper and lower mantle is assumed to correspond to a depth of 670 km. At the outer surface of the model we shall impose a lithosphere of variable thickness L in which the viscosity is infinite. Our purpose in analyzing the predicted $\dot{J}_2$ of this family of models is to establish that the model predictions are essentially insensitive to L (unlike the polar wander datum [*Peltier*, 1982; *Peltier and Wu*, 1983; *Wu and Peltier*, 1984]) and to the presence of any density increase across 670-km depth which might plausibly be ascribed to an increase of mean atomic weight. Since these are the physical features of the model which one might expect to produce the most extreme influence on the $\dot{J}_2$ prediction (aside from the viscosity structure), the explicit demonstration that the predictions are relatively insensitive to such variations confirms the LAGEOS datum as one which is particularly useful in constraining the relative viscosities of the upper and lower mantles. One additional sensitivity test which we shall perform concerns the effect on the $\dot{J}_2$ prediction of any boundary layer structure in the viscosity profile at 670-km depth which we would expect if there were a sufficiently large chemical increase of density across this level to prevent radial mass transfer. The double-layer mantle convective circulation which would obtain in this circumstance would have a strong thermal boundary layer at 670-km depth in which the temperature

Paper number 4B1057.
0148-0227/85/004B-1057$05.00

increased by at least 500°C from the upper into the lower mantle. This would be accompanied by the presence of a thin low-viscosity layer on the upper mantle side of the boundary and a thin high-viscosity layer (internal lithosphere) on the lower mantle side of the boundary. As we shall see, the $\dot{J}_2$ datum is also relatively insensitive to the presence of such an internal viscosity boundary layer structure.

The paper is organized in three main sections. The following two sections will review and extend the theory which has been developed to predict the rotational response to glacial forcing. The main extension of previously published theory is in the method employed to deduce the time domain form of the surface load Love number of degree 2, $k_2^L(t)$, which is fundamental to the analysis (section 3). In previous work the amplitudes of the discrete set of normal modes of viscous gravitational relaxation, in terms of which $k_2^L(t)$ is expressed, were computed using a collocation method. This has the undesirable feature that the amplitudes of the modes are not determined independently. Here we will show that it is possible to compute the modal amplitudes in a much more elegant fashion which does not suffer from this drawback. In section 4 of the paper this theory is employed to predict $\dot{J}_2$ for the previously discussed family of earth models and to establish the strength of the constraint on deep mantle viscosity which the LAGEOS observation provides. Our conclusions are summarized in section 5.

2. Theoretical Calculation of $\dot{J}_2$ and Associated "Nontidal" Acceleration of Rotation

Since the planet is subject to no net external torque during the changes of climate which accompany the accumulation and disintegration of Pleistocene ice sheets, the total angular momentum of the system is conserved. The time variations of system angular velocity are therefore described by the Euler equations

$$\frac{d}{dt}(J_{ij}\omega_j) + \varepsilon_{ijk}\omega_j J_{kl}\omega_l = 0 \tag{1}$$

in which J_{ij} is the (time dependent) moment of inertia tensor of the planet, $\boldsymbol{\omega}$ is the angular velocity vector, and ε_{ijk} is the Levi-Cevita (alternating) tensor. For sufficiently small perturbations away from an initial state of steady axial rotation with angular velocity Ω, (1) may be linearized with the following perturbation expansions:

$$\omega_i = \Omega(\delta_{i3} + m_i) \tag{2}$$

$$J_{ij} = I_{ij} \qquad i \neq j \tag{3a}$$

$$J_{11} = A + I_{11} \tag{3b}$$

$$J_{22} = A + I_{22} \tag{3c}$$

$$J_{33} = C + I_{33} \tag{3d}$$

Substituting (2) and (3) into (1), and dropping terms of second and higher order in the perturbations m_i and I_{ij}, decouples (1) into the following two independent equations:

$$\frac{i}{\sigma_r}\dot{\mathbf{m}} + \mathbf{m} = \boldsymbol{\psi} \tag{4}$$

$$\dot{m}_3 = \dot{\psi}_3 \tag{5}$$

In (4), $\sigma_r = \Omega(C - A)/A$ is the Chandler wobble frequency of the rigid earth and the vectors $\mathbf{m}$ and $\boldsymbol{\psi}$ are such that

$$\mathbf{m} = m_1 + im_2 \tag{6}$$

$$\boldsymbol{\psi} = \psi_1 + i\psi_2 \tag{7}$$

$$\psi_1 = \frac{I_{13}}{(C - A)} + \frac{\dot{I}_{23}}{\Omega(C - A)} \tag{8a}$$

$$\psi_2 = \frac{I_{23}}{(C - A)} - \frac{\dot{I}_{13}}{\Omega(C - A)} \tag{8b}$$

$$\psi_3 = -\frac{I_{33}}{C} \tag{8c}$$

Equation (4) describes the forced polar motion, while (5) describes the forced variation of the axial rate of rotation. Only the latter will concern us in this paper. A detailed recent analysis of the former effect will be found in the work of *Wu and Peltier* [1984]. In order to solve (5) we must be able to compute the perturbation of the axial component of inertia I_{33} which is produced by glacial loading and unloading.

In the domain of the Laplace transform variable s, the solution to (5) is simply

$$m_3(s) = -\frac{I_{33}(s)}{C} \tag{9}$$

For an arbitrary radially stratified viscoelastic earth, analysis by *Peltier* [1982] and *Wu and Peltier* [1984] shows that $I_{33}(s)$ may be written as

$$I_{33}(s) = [1 + k_2^L(s)]f(s)I_{33}^R \tag{10}$$

in which $k_2^L(s)$ is the Laplace transform domain form of the surface load Love number of degree 2, $f(s)$ is the Laplace transform of the loading history $f(t)$, and I_{33}^R is the perturbation of the axial component of inertia which would be produced by the changing surface ice and water load if the earth were rigid. As discussed in detail by *Wu and Peltier* [1984], I_{33}^R has a particularly simple form if we assume that during a glaciation-deglaciation cycle we may approximate the active ice sheets by circular disc loads of fixed radii α_i whose centroids are located at colatitudes θ_i and which accrete ice from and uniformly discharge their meltwater to, ocean basins of realistic shape. Under these assumptions, I_{33}^R may be expressed as

$$I_{33}^R = \sum_{i=1}^{M} M_i a^2 \left[\frac{2}{15}\frac{a_{20}}{a_{00}} - \frac{1}{3}\cos\alpha_i(1 + \cos\alpha_i)P_2^0(\cos\theta_i)\right] \tag{11}$$

In (11) the number $a_{20}/a_{00} = -0.1925$ is a ratio of spherical harmonic coefficients in the expansion of the "ocean function" which describes the shape of the ocean basins [e.g., *Lambeck*, 1980]. The M_i are the masses of each of the i ice sheets at glacial maximum and a is the earth's radius. The values of the parameters required to determine I_{33}^R for the three main centers of glaciation and deglaciation are listed in Table 1.

The influence of radial viscoelastic earth structure upon the predicted acceleration of rotation in (9) is entirely contained in

TABLE 1. Ice Sheet Parameters

	Laurentian	Fenoscandian	Antarctic
Mass M_i, kg × 10^{19}	2	0.56	0.70
Radius α_i, deg	15	9.5	20
Colatitude θ_i, deg	30	25.5	180
East longitude θ_i, deg	270	25.0	0
I_{33i}^R, × 10^{32} kg m^2	−3.420	−1.130	−1.799

the Love number $k_2{}^L(s)$. As shown by *Peltier* [1976], this Love number may be written in the form of a normal mode decomposition as

$$k_2{}^L(s) = k_2{}^{LE} + \sum_{j=1}^{N} \frac{r_j}{s + s_j} \tag{12}$$

where the s_j are the inverse relaxation times of the N normal modes of viscous gravitational relaxation required to synthesize the time domain behavior of the Love number of degree 2 and the r_j are the initial amplitudes for impulsive forcing. Parameter $k_2{}^{LE}$ is the elastic surface load Love number of degree 2. If we define the isostatic factor l_s as

$$l_s = \lim_{s \to 0} [1 + k_2{}^L(s)] \tag{13}$$

then since

$$\lim_{s \to 0} k_2{}^L(s) = k_2{}^{LE} + \sum_{j=1}^{N} \frac{r_j}{s_j} \tag{14}$$

we may rewrite (12) as

$$k_2{}^L(s) = (l_s - 1) - s \sum \frac{(r_j/s_j}{(s + s_j)} \tag{15}$$

Substituting $1 + k_2{}^L(s)$ from (15) into (10) and (10) into (9), Laplace inversion of $m_3(s)$ yields the formal solution for the forced increment of axial angular velocity as

$$m_3(t) = \frac{-I_{33}{}^R}{C} [D_1 f(t) + \sum_j r_j (f * e^{-s_j t})] \tag{16}$$

in which

$$D_1 = l_s - \sum \frac{r_j}{s_j} = 1 + k_2{}^{LE} \tag{17}$$

In (16) the asterisk denotes the convolution operation. The predicted acceleration of rotation is obtained from (16) by direct time differentiation which yields

$$\dot{m}_3(t) = \frac{\dot{\omega}_3}{\Omega} = \frac{-I_{33}{}^R}{C} \left[D_1 \dot{f}(t) + \sum r_j \frac{d}{dt} (f * e^{-s_j t}) \right] \tag{18a}$$

This is the theoretical solution on the basis of which all of the analyses discussed in this paper will depend. For the glaciation history $f(t)$ we will employ a seven-cycle sawtooth load history of the form shown in Figure 4 of *Wu and Peltier* [1984] in which each cycle of the periodic loading-unloading history has a slow linear glaciation phase lasting 90,000 years and a fast deglaciation phase of duration 10,000 years. The 10^5 years separating successive interglacials is well constrained by oxygen isotope data from deep sea sedimentary cores [e.g., *Broecker and Van Donk*, 1970; *Hays et al.*, 1976] as is the shape of individual glaciation pulses. Although we will demonstrate the sensitivity of our theoretical results to the timing of the glacial cycle, the $\delta^{18}O$ data from deep sea cores strongly constrain the time of the most recent and rapid ice sheet disintegration to 11,000 years B.P. ($\pm \sim 300$ years).

In order to compare our model predictions with the $\dot{J}_2$ inferred from LAGEOS orbital data, it is necessary to establish the connection between the nontidal acceleration $\dot{m}_3(t)$ and the parameter $\dot{J}_2$. As shown by *Peltier* [1982] and *Wu and Peltier* [1984] these two parameters are related as

$$\dot{J}_2(t) = \frac{-3C}{2m_e a^2} \cdot \dot{m}_3(t) \tag{18b}$$

All that remains is to specify the numbers r_j, s_j, $j = 1, 1, N$ for each of the earth models of interest to us. The main new theoretical development concerns this aspect of the calculation and is discussed in the following section.

3. COMPUTATION OF THE NORMAL MODE PARAMETERS r_j AND s_j

These parameters are obtained by analysis of the response of a radially stratified viscoelastic model of the earth to gravitational interaction with a mass load placed on its surface. The gravitationally induced deformation satisfies the usual equations for momentum conservation, conservation of mass, and for the deformation-induced perturbation of the gravitational potential. To first order in the small perturbations these equations are, respectively,

$$0 = \nabla \cdot \boldsymbol{\sigma} - (\rho g \mathbf{u} \cdot \hat{e}_r) - \rho \nabla \phi + g \nabla \cdot (\rho \mathbf{u}) \hat{e}_r \tag{19}$$

$$\rho' = -\nabla \cdot (\rho \mathbf{u}) \tag{20}$$

$$\nabla^2 \phi = 4\pi G \rho' \tag{21}$$

In the momentum equation (19) the inertial force has been neglected on the basis of the fact that we are concerned with describing processes whose characteristic time scales are sufficiently long that they are quasi-static. In (19), $\boldsymbol{\sigma}$ is the stress tensor, $\rho(r)$ and $g(r)$ are the background fields of density and gravitational acceleration, $\mathbf{u}$ is the displacement vector, and ϕ is the perturbation of the ambient gravitational potential. In the continuity equation (20), ρ' is the density perturbation and G in the Poisson equation (21) is the gravitational constant. In the domain of the Laplace transform variable s the above field equations continue to describe the dynamics and in this domain the constitutive relation which we employ to connect stress and strain has the form

$$\sigma_{ij}(s) = \lambda(s) e_{kk} \delta_{ij} + 2\mu(s) e_{ij} \tag{22}$$

with

$$\lambda(s) = \frac{\lambda s + \mu k/\nu}{s + \mu/\nu} \tag{23a}$$

$$\mu(s) = \frac{\mu s}{s + \mu/\nu} \tag{23b}$$

the appropriate frequency dependent moduli for a Maxwell solid (e.g., see *Peltier* [1974]). The second term in (19) is crucial for the correct description of postglacial rebound processes using the correspondence principle (e.g., see *Peltier* [1974]). This term describes the body force on the material which exists in consequence of the fact that the earth model is subject to a hydrostatic prestress prior to the time that internal deformation is induced by surface loading [*Love*, 1911]. Since this hydrostatic prestress is the pressure p and since $\partial p/\partial r = -\rho g$ it is clear that this extra body force is just the gradient of the radially advected prestress. It is through the presence of this term that internal density discontinuities in the interior of the model give rise to new modes of viscous gravitational relaxation since the term introduces an extra buoyancy force proportional to the density difference across the boundary and to the boundary displacement. Only when this term is included in the momentum equation [e.g., *Peltier*, 1974] can one directly apply the principle at correspondence to analyze the isostatic adjustment process using a normal mode formalism without having to make ad hoc adjustments to the boundary conditions across internal and exterior boundaries. This is an important point which is apparently not generally understood (e.g., *Nakiboglu and Lambeck* [1982]

do not include the prestress term and are led to assert that the correspondence principle cannot be directly applied to the viscoelastic relaxation problem).

We lose no important generality in seeking solutions to (19)–(21) which have the spheroidal symmetry

$$\mathbf{u} = \sum_{l=0}^{\infty} \left[U_l(r, s) P_l(\cos\theta)\hat{e}_r + V_l(r, s) \frac{\partial P}{\partial \theta}(\cos\theta)\hat{e}_\theta \right] \tag{24a}$$

$$\phi = \sum_{l=0}^{\infty} \phi_l(r, s) P_l(\cos\theta) \tag{24b}$$

$$\nabla \cdot \mathbf{u} = \sum_{l=0}^{\infty} X_l(r, s) P_l(\cos\theta) \tag{24c}$$

since we are interested in constructing the solution for point mass loading with $\delta(t)$ time dependence. Substitution of (24) into (19)–(21) reduces the set of coupled partial differential equations to a set of six simultaneous ordinary differential equations in the form

$$\frac{dY}{dr} = \mathbf{A}\mathbf{Y} \tag{25}$$

in which $\mathbf{A}$ is the matrix of coupling coefficients whose elements are listed in equation (3.12) of *Peltier* [1982]. For impulsive point mass forcing (25) is solved subject to the following boundary conditions which obtain for a point load of unit mass:

$$Y_3(a) = -g\frac{(2l+1)}{4\pi a^2} \tag{26a}$$

$$Y_4(a) = 0 \tag{26b}$$

$$Y_6(a) = -\frac{g}{m_e}(2l+1) \tag{26c}$$

where the elements of the solution six-vector $\mathbf{Y}$ are $\mathbf{Y} = (U_l, V_l, T_{rl}, T_{r\theta}, \phi_l, Q_l)$ in which

$$T_{rl} = \lambda X_l + 2\mu \dot{\mathbf{U}}_l \tag{27a}$$

$$T_{r\theta} = \mu\left(\dot{V}_l - \frac{1}{r}V_l + \frac{1}{4}\mathbf{U}_l\right) \tag{27b}$$

$$Q_l = \dot{\phi}_l + \frac{(l+1)}{r}\phi_l + 4\pi G_\rho \mathbf{U}_l \tag{27c}$$

It is at this point in the analysis that the theory will be considerably extended from that previously published (e.g., as reviewed by *Peltier* [1982]), since it is at this point that we must consider the problem of transforming the Laplace transform domain solution obtained by solving (25) subject to (26) back into the time domain. Previous analysis has been based upon a hybrid of the collocation method introduced by *Peltier* [1974] and the normal mode theory first presented by *Peltier* [1976]. Here we will develop a method which uses only normal mode analysis. As we will see, this method allows us to avoid several of the pitfalls which are inherent to the hybrid scheme.

Using the shooting algorithm discussed by *Peltier* [1974], the general solutions to (25) may be obtained in the form of a linear combination of three linearly independent solutions which satisfy the condition of regularity at $r = 0$. If we call these linearly independent solutions $\mathbf{T}_1$, $\mathbf{T}_2$, $\mathbf{T}_3$, then in general

$$\mathbf{Y}(r, s) = c_1(s)\mathbf{T}_1(r, s) + c_2(s)\mathbf{T}_2(r, s) + c_3\mathbf{T}_3(r, s) \tag{28}$$

If we denote the boundary conditions (26) by $\mathbf{B}(a, s)$, then the coefficients $c_i(s)$ are determined by

$$\mathbf{B}(s) = \mathbf{Y}(a, s) = c_1(s)T_1(a, s) + c_2(s)\mathbf{T}_2(a, s) + c_3(s)\mathbf{T}_3(a, s) \tag{29a}$$

For the impulse boundary conditions (26) the elements b_i of $\mathbf{B}$ are in fact s independent. If we define a vector $\mathbf{C}$ as

$$\mathbf{C} = [c_1(s), c_2(s), c_3(s)]$$

and denote by $\mathbf{M}$ the matrix whose column vectors are $\mathbf{T}_1(a, s)$, $\mathbf{T}_2(a, s)$, and $\mathbf{T}_3(a, s)$, then

$$\mathbf{B} = \mathbf{M}\mathbf{C} \tag{29b}$$

or

$$\mathbf{C} = \mathbf{M}^{-1}\mathbf{B} \tag{29c}$$

Now since $\mathbf{M}^{-1} = \mathbf{M}^*/\det\mathbf{M}$ where $\mathbf{M}^*$ is the transpose matrix of the cofactors M_{ij}^*, therefore

$$c_i = \sum_{j=1}^{3} \frac{M_{ij}^*(s) b_j}{\det \mathbf{M}} \tag{30}$$

and the solution satisfying the boundary conditions is

$$\mathbf{Y}(r, s) = \sum_{ij} \frac{M_{ij}^* b_j}{\det \mathbf{M}} \mathbf{T}_i(r, s) = \frac{Q(r, s)}{\det \mathbf{M}} \tag{31}$$

where $\mathbf{Q} = \sum_{ij} M_{ij}^* b_j \mathbf{T}_i$. Equation (31) now gives the general solution in a form which is useful for inversion. Suppose we define

$$\mathbf{Y}^V(r, s) = \mathbf{Y}(r, s) - \mathbf{Y}^E(r, s) = \frac{Q^V(r, s)}{\det \mathbf{M}} \tag{32}$$

where

$$\mathbf{Y}^E = \lim_{s \to \infty} \mathbf{Y}(r, s)$$

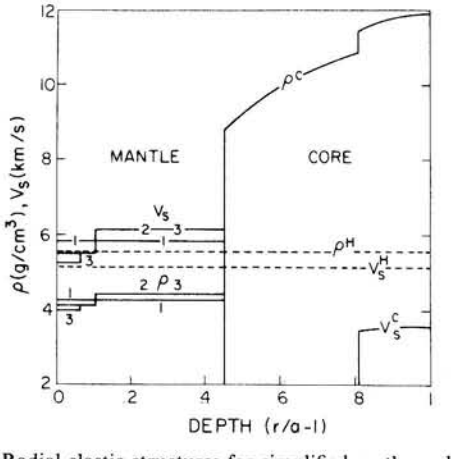

Fig. 1. Radial elastic structures for simplified earth models of the type analyzed in this paper. V_s is the shear wave velocity and ρ is the density. The dashed lines are representative average values of these parameters for the whole earth. Most of the analyses to be discussed employ models 1 or 2 which have constant mantle density and a single density discontinuity at 670-km depth, respectively. The effect of compressibility is included only in the lithosphere where the compression wave velocity V_p is taken equal to that in model 1066B of *Gilbert and Dziewonski* [1975].

The time domain form of the solution (31) may now be written as

$$\mathbf{Y}(r, t) = \frac{1}{2\pi i} \int_L \frac{Q^V(r, s)}{\det \mathbf{M}} e^{st}\, ds + \mathbf{Y}^E \delta(t) \tag{33}$$

where L is the Bromwich path. If s_j $(j = 1, N)$ are the zeros of the secular determinant det M, then (33) may be simply evaluated as

$$\mathbf{Y}(r, t) = \sum_{k=1}^{N} \text{Res} \left[\frac{Q^V(r, s)e^{st}}{\det \mathbf{M}(r, s)}; s_j \right] + \mathbf{Y}^E(r)\delta(t) \tag{34}$$

Since $d(\det \mathbf{M})/ds \neq 0$ in general at $s = s_j$, it follows that the residues at the poles s_j are

$$\text{Res} \left[\frac{Q^V(r, s)e^{st}}{\det \mathbf{M}(r, s)}; s_j \right] = \frac{Q^V(r, s_j)e^{s_j t}}{(d/ds)(\det \mathbf{M})|_{s=s_j}} \tag{35}$$

and therefore that

$$\mathbf{Y}(r, t) = \sum_{k=1}^{N} \frac{\mathbf{Q}^V(r, s_j)e^{s_j t}}{(d/ds)(\det \mathbf{M})} + \mathbf{Y}^E\delta(t) \tag{36}$$

If we define the vector of residues $\mathbf{R}_k$ as

$$\mathbf{R}_k = \frac{\mathbf{Q}^V(r, s_j)}{(d/ds)(\det \mathbf{M})|_{s=s_j}} \tag{37}$$

then

$$\mathbf{Y}(r, t) = \mathbf{Y}^E\delta(t) + \sum_{j=1}^{N} \mathbf{R}_j e^{-\bar{s}_j t} \tag{38}$$

where we have written $s_j = -\bar{s}_j$, since the N zeros of det M are all (usually) located on the negative real axis in the complex s plane. In the new normal mode solution for the residues (37) the r_j are inversely proportional to the slope of the secular function as it passes through zero at the location of the mode with inverse relaxation time s_j. The final solution (38) has exactly the same form as that obtained previously [e.g., *Peltier*, 1982] in that the time domain response to impulsive forcing is composed of an immediate elastic component $\mathbf{Y}^E$ and a viscous component which for each l (suppressed in deriving (38)) consists of the superposition of a discrete set of pure exponential relaxations. The surface load Love numbers $h_l^L(r, s)$, $l_l^L(r, s)$, and $k_l^L(r, s)$ are simply defined as

$$\begin{aligned} U_l(r, s) &= \phi_{1,l}(r) h_l^L(r, s)/g_0 \\ V_l(r, s) &= \phi_{1,l}(r) l_l^L(r, s)/g_0 \\ \phi_{2,l}(r, s) &= -\phi_{1,l}(r) k_l^L(r, s) \end{aligned} \tag{39}$$

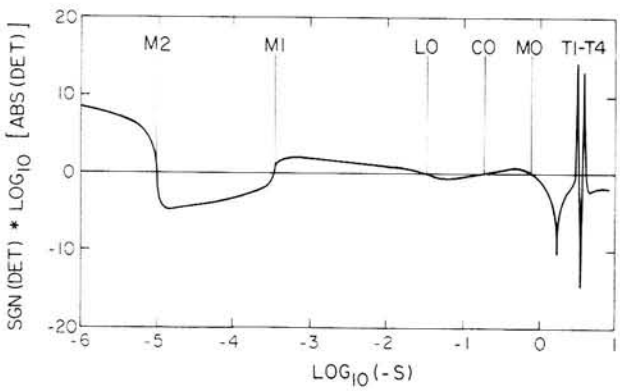

Fig. 2. The secular function det M for elastic model 3 of Figure 1 is shown as the dashed line labeled DET.

TABLE 2. Physical Parameters for Model 3

Region	ν, Pa s	ρ, kg m^{-3}	v_p, m s^{-1}	v_s, m s^{-1}
Core	0	...*	...*	...*
Lower mantle	10^{21}	4372	...	6117
Transition zone	10^{21}	4100	...	5475
Upper mantle	10^{21}	3959	...	5219
Lower lithosphere (>120.7 km)	∞	3959	9323	5219
Upper lithosphere (>21 km)	∞	3468	7781	3860

*Varying as shown in Figure 1 (same as 1066B).

in which g_0 is the surface gravitational acceleration and $\phi_{1,l}$ and $\phi_{2,l}$ are the spherical harmonic coefficients of the potential perturbation produced by the load and by the load-induced deformation, respectively. As seen in the analysis leading to (18), only the surface load Love number of degree 2, k_2^L is required in the solution for the acceleration of rotation induced by ice sheet loading and unloading. Since $\phi_{1,l} = ag_0/m_e$, where m_e is the earth's mass [see *Peltier*, 1982, equation 3.22], it is clear that the r_j in (12) are simply the suitably normalized elements of R_{5j}. We will proceed to provide an explicit comparison between the collocation method of calculating the r_j (see equation 3.31 of *Peltier* [1982]) and the normal mode method embodied in (37).

Figure 1 shows a sequence of illustrative radial elastic structures for the kind of earth models to which we will be confining our attention in this paper. Models are characterized by their radial density and shear wave velocity profiles and compressibility is included only in the lithosphere. Figure 2 shows the secular function det M as a function of s along the negative real s axis for elastic model 3 of Figure 1 in conjunction with a radial viscous structure in which the lithospheric thickness $L = 120.7$ km and for which the upper and lower mantle viscosities are $\nu_{UM} = 10^{21}$ Pa s and $\nu_{LM} = 10^{21}$ Pa s. The exact values of all of the model parameters are listed in Table 2. Note that the compressibility of the lithosphere is expressed in terms of a finite compression wave velocity V_p and that this region includes a lower density crust at the surface. Inspection of the degree 2 secular determinant for this model shown in Figure 2 shows that there are nine distinct modes of relaxation. The inverse relaxation times for these nine modes are tabulated in column 1 of Table 3 where the values of s have been nondimensionalized with a characteristic time of 10^3 years. This table also contains a comparison of modal strengths in terms of the number

$$\%\ \text{strength} = \frac{r_j/s_j}{\sum_j r_j/s_j} \tag{40}$$

which from (12) is just the ratio of the viscous relaxation carried by the jth mode to the total viscous relaxation in the degree 2 harmonic. The nine modes are named in column 1 using the mode-labeling procedure employed by *Peltier* [1976] in which the T modes are the so-called transition modes which all have relaxation times near the Maxwell time of the mantle and which are only weakly excited; the fundamental MO mode is supported by the density jump across the free outer surface of the model; CO, by that across the core mantle boundary; LO, by the infinite viscosity contrast between the lithosphere and mantle; and M1–M2, by the density jumps across the 670-km and 420-km seismic discontinuities

TABLE 3a. Comparison of Modal Excitation Strengths Using the Normal Mode (New) and Collocation (Old) Methods for Earth Mode 3 and h_2^L

Mode	s ($[T] = 10^3$ yr)	% Strength (New or Old)	% Strength (Old, 7 Modes)	% Strength (Old 5 Modes)
T4	−3.8165	0.3	...	...
T3	−3.7135	0.0	...	...
T2	−3.3422	0.4	1.2	...
T1	−3.0913	0.1	−0.5	...
M0	-7.1861×10^{-1}	42.9	42.9	45.1
C0	-1.7938×10^{-1}	22.8	22.8	19.8
L0	-5.3947×10^{-2}	21.8	21.8	23.8
M1	-2.9019×10^{-4}	10.4	10.4	9.4
M2	-8.0197×10^{-6}	1.4	1.4	2.3
Total		100.0	100.0	100.4

which mark the bottom and top of the transition zone, respectively. These latter modes will of course exist only to the extent that the discontinuities to which they correspond in the real earth are capable of producing a buoyancy force when they are deflected from their equilibrium levels. This will certainly be the case if the boundaries are of chemical origin or if they are due to solid-solid phase transitions for which the reaction rates are slow on the time scale of the relaxations which they support. To the extent that the candidate phase transitions are known to have fairly fast reaction kinetics (i.e., are observable over "human" time scales in the laboratory), we might be tempted to view the requirement that an M1 or M2 mode exist as direct evidence that the associated boundary is in some substantial part a chemical one. It turns out, however, that even if the 420-km and 670-km discontinuities are due entirely to equilibrium phase transformations, they will behave as if they were chemical discontinuities on the time scales of the glacial isostatic adjustment process to the extent that they may be considered invariant (e.g., see *Peltier* [1985] and references therein).

Intercomparison of the percent strength data in Tables 3a and 3b (Table 3a shows results for the Love number h_2^L while Table 3b shows results for the Love number k_2^L) for the various calculations shown demonstrates several interesting features. The first point to notice (from column 3) is that the old and new methods give identical results when all of the modes are employed. The data in column 5 shows that if the set of transition modes are neglected, which might seem reasonable since they have small percent strength, the old collocation method makes significant errors in partitioning the total relaxation among the physically important modes. Keeping only two of the four transition modes (column 4) leads to large errors in the percent strength computed for the transition modes retained, but the errors for the remaining modes are small. The main advantage of the new method, assuming that all of the normal mode poles have been found, is therefore that it delivers an accurate value for the residue at a given pole which is independent of those at all other poles. In the collocation calculation (e.g., equation 3.31 of *Peltier* [1982]), on the other hand, the r_j are strongly interdependent. Clearly, if we propose to detect the presence or absence of chemical heterogeneity in the mantle by attempting to prove that some particular geophysical observation (say, free air gravity) requires the presence of the M1 mode (say), then we require an accurate method of computing the relative strength of this mode in the relaxation spectrum. The new normal mode method derived here has the required accuracy for this purpose. In the next section we will apply this method to the analysis of the constraints on viscoelastic earth structure provided by the LAGEOS ranging data.

TABLE 3b. Same as Table 3a but for Love Number 2 k_2^L

Mode	s	% Strength (New or Old)	% Strength (Old, 7 Modes)	% Strength (Old 5 Modes)
T4	3.8165	0.4	...	...
T3	3.7135	0.0	...	...
T2	3.3422	0.4	1.6	...
T1	3.0913	0.2	−0.6	...
M0	7.1861×10^{-1}	55.1	55.2	58.0
C0	1.7938×10^{-1}	23.1	23.1	19.4
L0	5.3948×10^{-2}	17.8	17.8	20.4
M1	2.9019×10^{-4}	2.7	2.7	1.5
M2	8.0197×10^{-6}	0.2	0.2	1.4
Total		100.0	100.0	100.6

4. Results of the Sensitivity Analyses

In this section we will explore the extent to which the viscosity of the lower mantle inferred from LAGEOS orbital observations may be obscured through dependence of the model predictions of $\dot{J}_2$ on parameters other than ν_{UM} and ν_{LM}. Previous analyses of this datum [*Peltier*, 1982, 1983; *Peltier and Wu*, 1983; *Wu and Peltier*, 1984] were all based upon models with 1066B elastic structure [*Gilbert and Dziewonski*, 1975] in which the 420- and 670-km seismic discontinuities were treated as boundaries capable of inducing a buoyant restoring force when they are deflected from their equilibrium levels by surface loading. If these boundaries were equilibrium phase boundaries for which the reaction kinetics are fast on the timescale of the viscous relaxation, they would clearly not be capable of inducing such buoyancy upon deflection. The M2 (420 km) and M1 (670 km) modes would therefore not exist. The question then arises as to whether the bounds previously obtained on ν_{LM} might not be drastically altered if the parameter were inferred using a model with no internal buoyancy in the mantle. This is only one of the several possible tradeoffs between the various parameters of the model which we will explore in what follows.

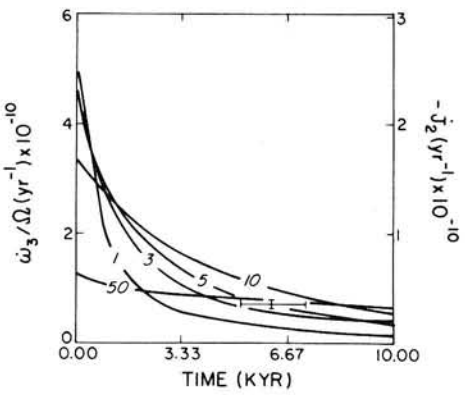

Fig. 3. The predicted nontidal acceleration $(\dot{\omega}_3/\Omega)$ and $\dot{J}_2$ as a function of time following deglaciation. The zero of time is at the end of the last 10^4 yr deglaciation phase of the cyclic load history. All calculations employ elastic model 1 of Figure 1 in conjunction with a surface lithosphere of thickness 120.7 km and a constant upper mantle viscosity $\nu_{UM} = 10^{21}$ Pa s. The numbers adjacent to each curve denote the multiplicative factor F in the lower mantle viscosity $\nu_{LM} = F \times 10^{21}$ Pa s. The cross at $t = 6$ kyr denotes the LAGEOS observation of $\dot{J}_2 = (-3.5 \pm 0.3) \times 10^{-11}$ yr^{-1}.

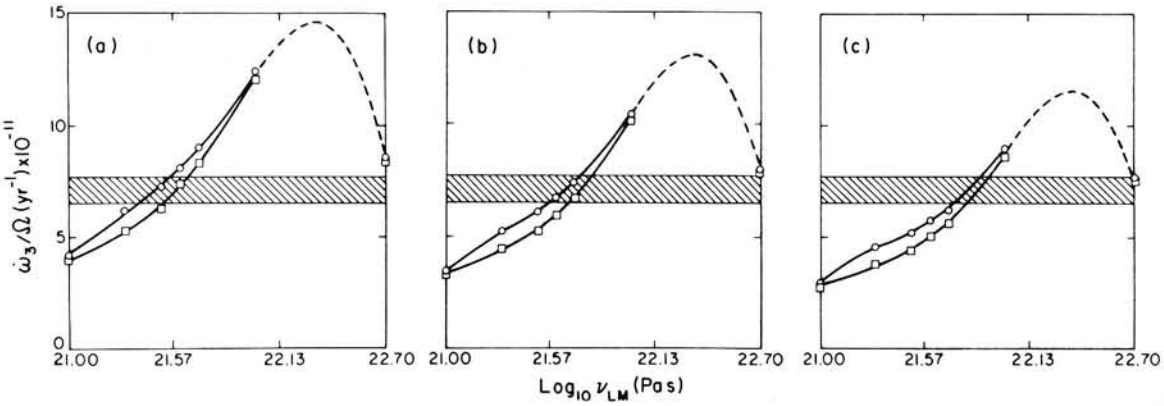

Fig. 4. Predicted $\dot{\omega}_3/\Omega$ and $\dot{J}_2$ as a function of the lower mantle viscosity ν_{LM}. Figures 4*a*, 4*b*, and 4*c* show $\dot{J}_2$ versus ν_{LM} for the choices $t = 5$ kyr, 6 kyr, 7 kyr, respectively, for the time of the current epoch of observation measured with respect to the end of the last glacial cycle. The open circles show the results for models which have no internal density discontinuities in the mantle and no boundary layer structure in the viscosity field at 670-km depth. The open squares show results for a model which has a perfectly elastic layer (an internal lithosphere) of thickness 50 km immediately beneath the 670-km seismic discontinuity.

4.1. *Bounds on ν_{LM} From a Model With No Internal Mantle Buoyancy*

The first set of calculations we shall describe employ elastic model 1 of Figure 1 which has no internal density discontinuities in the mantle. The lithospheric thickness is fixed at $L = 120.6$ km, and it is treated as compressible with compression wave velocity V_p equal to that over the same range of depth in model 1066B. The upper mantle viscosity is fixed at $\nu_{UM} = 10^{21}$ Pa s. Figure 3 shows the model predictions (from (18*a*) and (18*b*)) of $\dot{\omega}_3/\Omega$ and $\dot{J}_2$ as a function of time following the end of the last of the 10^5 year model glaciation cycles. Predictions are shown for a sequence of models which differ only in ν_{LM}, and the observation of *Yoder et al.* [1983] is shown as the cross. The length of the vertical error bar is fixed by the experimental error of $\pm 0.3 \times 10^{-11}$ yr^{-1} for the $\dot{J}_2$ observation (note, however, that Yoder et al. imply the systematic error to be larger than this). The horizontal bar is of length 2 kyr and represents the range of times to which the present epoch could conceivably correspond in the context of the sawtooth model of the individual glaciation pulses which we are employing. On Figure 3 the observation is shown centered at a time of 6 kyr following the end of the final model deglaciation phase. This provides a best fit to the δ^{18}O chronology [*Peltier*, 1982]. Inspection of Figure 3 shows that there are two ranges of lower mantle viscosity with which it is possible to fit the data, just as was shown to be the case by *Peltier* [1983].

This fact is made clear by the presentation of the data in Figure 4. Figures 4*a*, 4*b*, and 4*c* show the predicted $\dot{\omega}_3/\Omega$ and $\dot{J}_2$ as function of ν_{LM} for three different choices of the present epoch from the end of the last model deglaciation phase. Figures 4*a*, 4*b*, and 4*c* are for the times $t = 5$ kyr, $t = 6$ kyr, and $t = 7$ kyr, repsectively, and cover the plausible range of choices for this time. On each panel the range of the observation is illustrated by the hatched region and the curve marked by the open circles shows the results of interest to us in this subsection. Analysis of these data shows that with the choice $t = 5$ kyr the bounds on ν_{LM} are 2.29×10^{21} Pa s $\leq \nu_{LM} \leq 3.55 \times 10^{21}$ Pa s, whereas with $t = 6$ kyr (the preferred time) we obtain 3.64×10^{21} Pa s $\leq \nu_{LM} \leq 5.23 \times 10^{21}$ Pa s, and finally with $t = 7$ kyr the result is 5.36×10^{21} Pa s $\leq \nu_{LM} \leq 7.13 \times 10^{21}$ Pa s. As discussed by *Peltier* [1983] the higher viscosity root near $\nu_{LM} = 10^{23}$ Pa s is completely ruled out by relative sea level and free air gravity observations. Since the preferred time is very close to $t = 6$ kyr on the basis of δ^{18}O data from deep sea sedimentary cores, it is clear that the bounds on ν_{LM} obtained with the earth model that has no internal mantle buoyancy are rather close to those obtained previously with an earth model with 1066B elastic structure. Apparently the $\dot{J}_2$ datum is relatively insensitive to the presence of internal mantle buoyancy and thus would not be useful in attempting to directly infer the presence or absence of chemical density discontinuities (or sluggish phase boundaries) in the earth. On the other hand, this insensitivity is precisely what makes the observation so important insofar as the internal viscosity stratification is concerned. We will illustrate the degree of insensitivity quantitatively in what follows.

4.2. *Sensitivity of the $\dot{J}_2$ Prediction to the Presence of Internal Density Discontinuities in the Mantle*

Figure 5 shows the percentage difference between the $\dot{J}_2$ predicted by a model with a density increase of 6.2% across 670-km depth and that for the homogeneous density model employed in the last subsection. The former corresponds to elastic model 2 in Figure 1. Inspection of the data in Figure 6

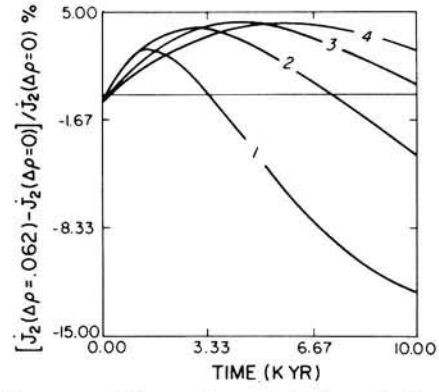

Fig. 5. Percentage difference between the $\dot{J}_2$ predictions of models with and without an internal density discontinuity at 670-km depth in the mantle (i.e., comparing results for elastic models 1 and 2 of Figure 1). The differences are shown as a function of time and for several different values of the lower mantle viscosity $\nu_{LM} = F \times 10^{21}$ Pa s. The numbers adjacent to each curve are the corresponding values of F.

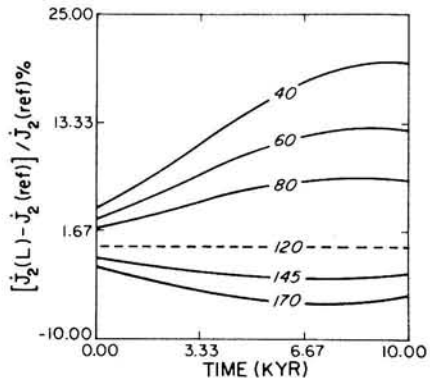

Fig. 6. Percentage difference between the $\dot{J}_2$ predictions of models which differ from one another only in lithospheric thickness. The reference model from whose predictions the deviations are computed is elastic structure 3 of Figure 1 with fixed viscosity values of $\nu_{UM} = 10^{21}$ Pa s and $\nu_{LM} = 4.5 \times 10^{21}$ Pa s. The different lithospheric thicknesses of the comparison models are marked adjacent to each curve.

shows that the difference in $\dot{J}_2$ between the two models vary from a value of -10% at long times for the model with $\nu_{LM} = 10^{21}$ Pa s to a value of $+5\%$ at intermediate times for the model with $\nu_{LM} = 4 \times 10^{21}$ Pa s. The number plotted is

$$P = [\dot{J}_2(\nabla\rho/\rho = 6.2\%)] - \dot{J}_2(\nabla\rho/\rho = 0)/\dot{J}_2(\nabla\rho = 0)$$

so that the presence of nonzero internal $\nabla\rho$ in the mantle increases the predicted $\dot{J}_2$ at small times but reduces it at later times. Near the preferred time of $t = 6$ kyr for the epoch of observation (now) the variation is only $\pm 5\%$. Since the observational error in $\dot{J}_2$ is $\pm 10\%$, it is clear that the effects of plausible variations of density across the 670-km discontinuity upon the prediction of the model is negligibly weak in comparison with the effect of plausible variations of mantle viscosity, even when these are confined entirely to the lower mantle.

4.3. *Sensitivity of the $\dot{J}_2$ Prediction to the Thickness and Nature of the Surface Lithosphere*

Inspection of (18*a*) shows that the influence of lithospheric thickness upon the $\dot{J}_2$ prediction is liable to be weak. This is due to the fact that the present epoch is one in which $f(t) = \dot{f}(t) = 0$ and thus the first term in brackets on the right-hand side of (18*a*) does not contribute to the prediction. This eliminates the explicit dependence on l_s (the isostatic factor) and thus any direct influence of lithospheric thickness. This expectation of weak dependence of $\dot{J}_2$ on L is born out by the results shown in Figure 6, which shows $P = [\dot{J}_2 - \dot{J}_2(L = 120.7 \text{ km})]/\dot{J}_2(L = 120.7 \text{ km})$ for several different lithospheric thicknesses between 40 km and 170 km. The basic model from whose predictions the deviations are computed is one for which $\nu_{LM} = 4.5 \times 10^{21}$ Pa s and which has the elastic structure of model 3 in Figure 1. The sensitivity of the $\dot{J}_2$ observation on this property of the earth is so weak (deviations less than 7% at all times for geophysically plausible models with 80 km $\leq L \leq$ 170 km) that no significant contamination of the ν_{LM} inference due to lack of knowledge of L is possible. This property of the $\dot{J}_2$ observation makes it a rotational response to glaciation which is strikingly different from the glaciation-induced polar motion which is extremely sensitive to L [*Peltier*, 1982; *Peltier and Wu*, 1983; *Wu and Peltier*, 1984].

Although the $\dot{J}_2$ predictions are relatively insensitive to lithospheric thickness, they are moderately more sensitive to the nature of the lithosphere employed in the calculation insofar as its compressibility or incompressibility is concerned. Figure 7*a* shows predicted $\dot{J}_2$ time histories for a sequence of models which differ only in lower mantle viscosity and which have an incompressible lithosphere of thickness 120.7 km. In Figure 7*b* the number $P = [\dot{J}_2(\text{compressible})] - \dot{J}_2(\text{incompressible})/\dot{J}_2(\text{incompressible})$ is shown as a function of time for the same sequence of models. At the preferred time $t = 6$ kyr the maximum deviation is for the model with $\nu_{LM} = 10^{21}$ Pa s and is in the amount of 18%. In general the effect of lithospheric compressibility is to slightly reduce the predicted $\dot{J}_2$ at short times and to increase it at later times. Although the sensitivity of the $\dot{J}_2$ prediction to this effect is not significant in comparison with that of variations of ν_{LM} we have nevertheless employed compressible lithospheres for all of the reference calculations in this paper. There do exist geophysical observations, however, such as the relative sea level data peripheral to the Laurentian ice sheet [*Peltier*, 1984] which are very sensitive to this feature of the model.

4.4. *Sensitivity of the $\dot{J}_2$ Prediction to the Presence of Boundary Layer Structure in the Viscosity Profile Across 670-km Depth*

One last sequence of analyses which we will discuss in this paper concerns the effects on the $\dot{J}_2$ prediction which should be expected as a consequence of the viscosity depth profile which would accompany the existence of a layered convective circulation in the earth's mantle. If mass transfer across the seismic discontinuity at 670-km depth were inhibited by a sharp increase of mean atomic weight or some as yet incom-

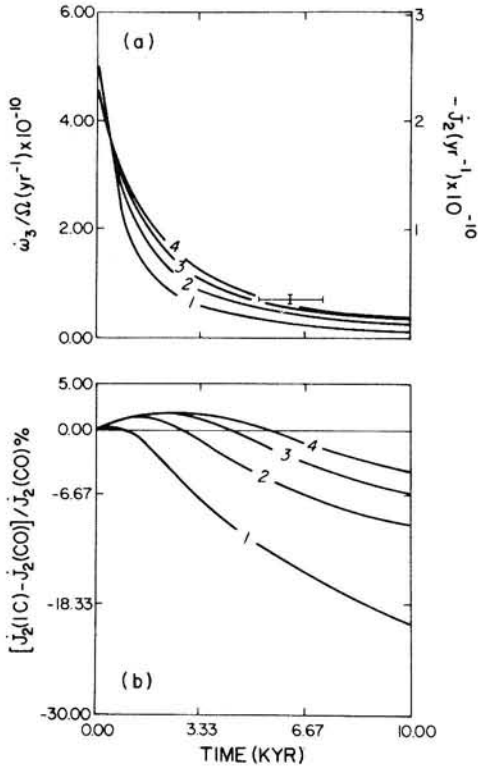

Fig. 7. (*a*) Predicted $\dot{J}_2$ and $\dot{\omega}_3/\Omega$ time histories for a sequence of models which have $\nu_{UM} = 10^{21}$ Pa s and $\nu_{LM} = F \times 10^{21}$ Pa s where the number F is marked adjacent to each curve. These models differ from the previous ones in that the lithosphere is treated as incompressible rather than compressible. (*b*) Time variations between the $\dot{J}_2$ predictions in Figure 7*a* and those for an otherwise identical control model whose lithosphere is compressible.

pletely understood effect of a phase boundary, then a thermal boundary layer would develop there through which the radial heat transfer was entirely effected by thermal diffusion (e.g, see *Peltier and Jarvis* [1982]). This layer would have a thickness comparable to that of the surface lithosphere, that is, of the order of 100 km, and the temperature increase would be of the order of $500°–10^3$ °C to satisfy the heat flow requirement. In the absence of any significant modification of the basic creep mechanism across the interface, we would expect the sharp increase of temperature to give rise to a sharp decrease of viscosity by perhaps 2–3 orders of magnitude. That this decrease of viscosity is not observed may be construed as an argument that no such boundary layer exists [*Peltier and Jarvis*, 1982]. However, this argument is not definitive, since the decrease of viscosity expected on the basis of the sharp temperature rise could be masked by an increase of creep activation energy or by effects due to change of crystal structure from the less dense to the more dense phase. Some such effect would be required to reconcile the viscosity profile required by the LAGEOS data with that expected in the layered convection scenario.

Even if such physical effects did exist which acted in such a way as to offset the expected general decrease of viscosity across the boundary layer due to the influence of temperature, there would still exist strong local variations of viscosity through the boundary layer itself. Clearly, the hot lower boundary layer of the upper mantle convective circulation would be a region of anomalously high viscosity compared with the overlying upper mantle, whereas the cold upper thermal boundary layer of the lower mantle convective circulation would be a region of anomalously high visosity compared with the underlying lower mantle. Across the boundary itself there would therefore exist a viscosity dipole such as that sketched in Figure 8. Figure 8*a* illustrates the modest and monotonic increase of viscosity which we would expect [*Peltier and Jarvis*, 1982] if the temperature change across 670-km depth were adiabatic, while Figure 8*b* illustrates the dipolar variation of viscosity which would accompany the presence of a thermal boundary layer at this depth when the creep activation energy increases by an amount adequate to offset the sharp decrease of viscosity which would otherwise be produced by the influence of temperature alone.

In the layered convection scenario, there are good dynamic reasons to believe that the dipolar viscosity variation through the 670-km discontinuity would be quite strongly asymmetric

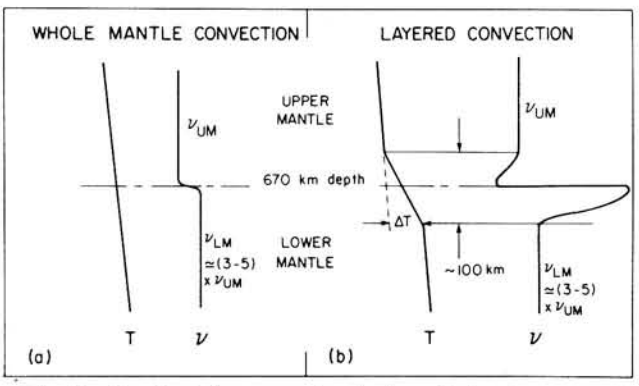

Fig. 8. Sketch of the expected variations of viscosity across the 670-km seismic discontinuity (*a*) if the temperature variation is adiabatic and (*b*) if the temperature profile includes a sharp thermal boundary layer.

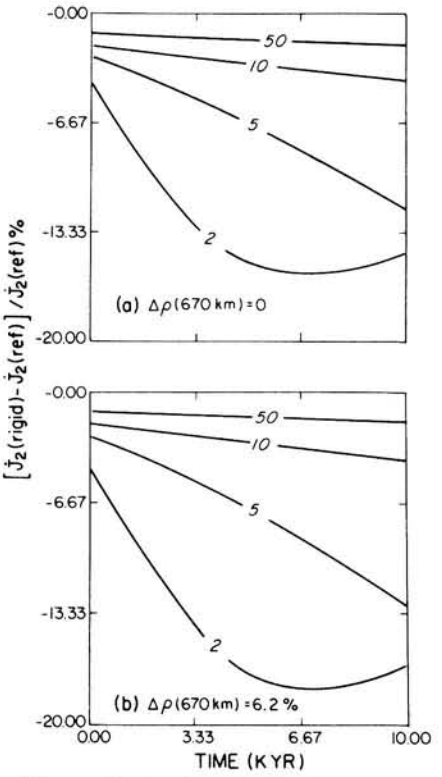

Fig. 9. Difference in the $\dot{J}_2$ predictions between models which have a rigid 50-km-thick lithosphere at 670-km depth and those which do not. The numbers adjacent to each curve are the value of F in the expression for the lower mantle viscosity $\nu_{LM} = F \times 10^{21}$ Pa s; $\nu_{UM} = 10^{21}$ Pa s is fixed. Figure 9*a* shows the comparison for models in which the $\nabla\rho$ across the 670-km boundary is zero and Figure 9*b* is for $\nabla\rho(670\text{ km}) = 6.2\%$.

(as sketched in Figure 8*b*). This asymmetry would be such that the low-viscosity region would be much less dramatically evident than would the high-viscosity region. This is basically because the low-viscosity region at the base of the upper mantle "layer" would be susceptible to a local convective instability which would tend to eliminate this low-viscosity component of the dipolar structure. In the limit in which such local instabilities are sufficiently vigorous to completely remove this region, the net effect on the viscosity profile of convective layering would be the presence of a high-viscosity "internal lithosphere" on the underside of the 670-km discontinuity. We will suppose that this internal lithosphere has a thickness of 50 km and an infinite viscosity and test the extent to which such a feature might influence the $\dot{J}_2$ prediction. This parameterization of the expected local effects on the radial viscosity profile of a layered convective circulation is clearly an extreme parameterization in the sense that the effects of a perfectly elastic internal lithosphere will be greater that those which would be produced by any plausible finite viscosity dipolar structure.

Figure 9 shows the percentage difference between the speed prediction for models with no internal elastic lithosphere and those including this feature. Figures 9*a* and 9*b* show the variation for models with constant mantle density and for models which have a density increase of 6.2% across 670-km depth, respectively. The number plotted on each frame is $[\dot{J}_2(\text{internal lithosphere}) - \dot{J}_2(\text{no lithosphere})]/\dot{J}_2(\text{no lithosphere})$ so that the effect of the presence of the internal lithosphere is to decrease the speed prediction, with the greater effect evident for

models with lowest lower mantle viscosity as expected on physical grounds. Comparison of Figures 9*a* and 9*b* shows that the presence or absence of a density jump at 670-km depth has no substantial influence on the nature of the variations produced by the presence of the internal lithosphere. The magnitude of the changes in $\dot{J}_2$ due to the presence of the internal layer ($\sim 10\%$ at the preferred time $t = 6$ kyr for modest ν_{LM}) is sufficiently large that we should be interested in the extent to which the presence of such a feature might influence the inferred value of ν_{LM} from the LAGEOS orbital data.

This influence on the inferred value of the lower mantle viscosity is analyzed in Figure 4, where, in each of the three panels (for the three previous choices of model t for the present epoch), we show the present-day $\dot{J}_2$ prediction as a function of lower mantle viscosity ν_{LM}. The predictions for models which include the "internal lithosphere" are marked with the square symbols. Inspection of these data shows that the value of ν_{LM} inferred on the basis of models which include an internal lithosphere is somewhat higher than that derived on the basis of models which have no such feature. The new bounds on ν_{LM} obtained with the choice of the present epoch as $t = 6$ kyr are 4.48×10^{21} Pa s $\leq \nu_{LM} \leq 5.95 \times 10^{21}$ Pa s. These compare with the old bounds of 3.64×10^{21} Pa s $\leq \nu_{LM} \leq 5.23 \times 10^{21}$ Pa s. Although the effect is not large, it is discernible. Of all the sensitivity tests which we have performed, it is the only one which has uncovered an effect which impacts substantially on the $\dot{J}_2$ prediction. The observation of $\dot{J}_2$ with the LAGEOS satellite has therefore provided us with an extremely important constraint on the relative viscosities of the upper and lower mantles.

5. CONCLUSIONS

In this paper we have analyzed the variations of earth's rate of rotation forced by the final retreat of Würm-Wisconsin ice which occurred between 18,000 and 6000 years ago. On the basis of the assumption that no significant variations of surface load have since taken place, the present-day nontidal acceleration is simply explained as a consequence of the delayed viscoelastic relaxation of the earth following deglaciation. A particularly simple set of layered viscoelastic models has been employed to fit the LAGEOS determination of $\dot{J}_2$ and the associated nontidal acceleration $\dot{\omega}_3/\Omega$. These models were characterized by the four parameters L, ν_{UM}, ν_{LM}, and $\nabla\rho$ (670) which are the thickness of the lithosphere, the upper and lower mantle viscosities, and the density increase across the seismic discontinuity at 670-km depth, respectively. In all of the $\dot{J}_2$ calculations which we have performed the upper mantle viscosity has been held fixed to the nominal value $\nu_{UM} = 10^{21}$ Pa s, which is well constrained by relative sea level data [*Peltier*, 1982].

Of the remaining three parameters, the model predictions are most sensitive to variations of ν_{LM}. With $\nabla\rho(670) = 0$ and $L = 120.7$ km, the LAGEOS value of $\dot{J}_2 = (-3.5 \pm 0.3) \times 10^{-11}$ yr^{-1} is fit within the experimental error by 3.6×10^{21} Pa s $\leq \nu_{LM} \leq 5.2 \times 10^{21}$ Pa s. This is to be compared with the allowed range of 2.7×10^{21} Pa s $\leq \nu_{LM} \leq 4.4 \times 10^{21}$ Pa s deduced by *Peltier* [1983] on the basis of models with elastic structure 1066B. This is very close agreement given the significant differences between the elastic structures employed in this paper and the seismically realistic structure 1066B. The implied lack of sensitivity of the $\dot{J}_2$ prediction to fairly substantial variations of the elastic structure has been explicitly demonstrated in a sequence of calculations in which L and $\nabla\rho(670)$ are varied over geophysically plausible ranges. Although neither of these effects is sufficiently strong to significantly modify the inference of ν_{LM} on the basis of the LAGEOS number for $\dot{J}_2$, it seems that the compressibility of the lithosphere is sufficiently important to warrant accounting for it in the analysis.

The only physical effect analyzed in this paper which was found to substantially modify the ν_{LM} inferred from the orbital data was that due to strong boundary layer structure in the viscosity profile at 670-km depth such as would accompany a layered mantle convective circulation. Using the most extreme form of this boundary layer structure, in which the cold upper boundary layer of the lower mantle convective circulation is represented by a perfectly elastic layer of 50-km thickness, we found that the ν_{LM} which was then inferred from the LAGEOS data was such that 4.48×10^{21} Pa s $\leq \nu_{LM} \leq 5.95 \times 10^{21}$ Pa s. This is to be compared with the previous range 3.64×10^{21} Pa s $\leq \nu_{LM} \leq 5.23 \times 10^{21}$ Pa s. Since the rigid layer parameterization of the expected boundary layer structure is extreme, the variation in the inferred value of ν_{LM} is the largest which might conceivably be produced by such a structure. Thus even if the mantle convective circulation were layered, the expected sharp local variations of viscosity at 670-km depth do not significantly modify the number inferred for the average viscosity of the lower mantle using the LAGEOS data.

The fact that the LAGEOS inference of ν_{LM} is not substantially contaminated by plausible changes of L and $\nabla\rho(670)$ is especially important because other signatures of glacial isostatic adjustment, such as the wander of the rotation pole [e.g., *Peltier and Wu*, 1983; *Peltier*, 1982; *Wu and Peltier*, 1984], are very sensitive to changes of all of these model parameters. In order to infer all of the parameters accurately, we must rely upon the fact that each of the signatures of isostatic adjustment has a different dependence on the various properties of the model. The four main signatures and their principal dependencies are as follows: (1) relative sea level data (Laurentian) inside the ice margin (ν_{UM}, (ν_{LM})) and outside the ice margin (ν_{UM}, L, (ν_{LM})); (2) $\dot{J}_2$ and the nontidal acceleration (ν_{UM}, ν_{LM}); (3) the free air gravity anomaly (ν_{UM}, ν_{LM}, $\nabla\rho(670)$); (4) true wander of the rotation pole (ν_{UM}, ν_{LM}, L, $\nabla\rho(670)$). The effort of which this paper is part is an attempt to exploit these differential dependencies to tightly constrain the four parameters (ν_{UM}, ν_{LM}, L, $\nabla\rho(670)$). The last of these four parameters is especially important because of the possibility that the requirement of a specific nonzero $\nabla\rho(670)$ may be directly construed as the requirement for chemical heterogeneity between the upper and lower mantle such as would almost certainly be required to induce a layered convective circualtion. As previously argued by *Peltier and Wu* [1982], the free air gravity data do seem to require the presence of an M1 mode. It is clear from point 3 above, however, that we will not be able to use the observed free air gravity anomalies to infer $\nabla\rho(670)$ unless we have independent constraints on ν_{UM} and ν_{LM}. The geodynamic importance of the LAGEOS data is that they have provided us with a tight constraint on ν_{LM}.

Acknowledgments. I am very much indebted to Rosemary Drummond and Atul Nautayal for their assistance in completing the computations described in this paper. Research support was from NSERC grant A9627.

REFERENCES

Alexander, J. C., Higher harmonic effects of the earth's gravitational field from postglacial rebound as observed by LAGEOS, *Geophys. Res. Lett.*, *10*, *1085–1087*, 1983.

Broecker, W. S., and J. Van Donk, Insolation changes, ice volumes,

and the O^{18} record in deep sea cores, *Rev. Geophys., 8*, 169–198, 1970.

Gilbert, F., and A. M. Dziewonski, An application of normal mode theory to the retrieval of structural parameters and source mechanisms from seismic spectra, *Philos. Trans. R. Soc. London Ser. A, 278*, 187–269, 1975.

Hays, J. D., J. Imbrie, and N. J. Swackleton, Variations in the earth's orbit: Pacemaker of the ice ages, *Science, 194*, 1121–1132, 1976.

Lambeck, K., *The Earth's Variable Rotation: Geophysical Causes and Consequences*, Cambridge University Press, New York, 1980.

Love, A. E. H., *Some Problems of Geodynamics*, Cambridge University Press, London, 1911. (Reprinted by Dover, New York, 1967.)

Nakiboglu, S. M., and K. Lambeck, A study of the earth's response to surface loading with application to Lake Bonneville, *Geophys. J. R. Astron. Soc., 70*, 577–620, 1982.

Peltier, W. R., The impulse response of a Maxwell earth, *Rev. Geophys., 12*, 649–669, 1974.

Peltier, W. R., Glacial isostatic adjustment, 2, The inverse problem, *Geophys. J. R. Astron. Soc., 46*, 669–706, 1976.

Peltier, W. R., Dynamics of the ice age earth, *Adv. Geophys., 24*, 1–146, 1982.

Peltier, W. R., Constraint on deep mantle viscosity from LAGEOS acceleration data, *Nature, 304*, 434–436, 1983.

Peltier, W. R., The thickness of the continental lithosphere, *J. Geophys. Res., 89*, 11,303–11,316, 1984.

Peltier, W. R., Mantle convection and viscoelasticity, *Annu. Rev. Fluid Mech., 17*, in press, 1985.

Peltier, W. R., and G. T. Jarvis, Whole mantle convection and the thermal evolution of the earth, *Phys. Earth Planet. Inter., 29*, 281–304, 1982.

Peltier, W. R., and P. Wu, Mantle phase transitions and the free air gravity anomalies over Fennoscandia and Laurentia, *Geophys. Res. Lett., 9*, 731–734, 1982.

Peltier, W. R., and P. Wu, Continental lithospheric thickness and deglaciation induced true polar wander, *Geophys. Res. Lett., 10*, 181–184, 1983.

Rubincam, D. P., Postglacial rebound observed by LAGEOS and the effective viscosity of the lower mantle, *J. Geophys. Res., 89*, 1077–1087, 1984.

Wu, P., and W. R. Peltier, Glacial isostatic adjustment and the free air gravity anomaly as a constraint on deep mantle viscosity, *Geophys. J. R. Astron. Soc., 74*, 377–450, 1983.

Wu, P., and W. R. Peltier, Pleistocene deglaciation and the earth's rotation: A new analysis, *Geophys. J. R. Astron. Soc., 76*, 753–792, 1984.

Yoder, C. F., J. G. Williams, J. O. Dickey, B. E. Schultz, R. J. Eanes, and B. D. Tapley, Secular variation of earth's gravitational harmonic J_2 coefficient from LAGEOS and nontidal acceleration of earth rotationn *Nature, 303*, 757–762, 1983.

W. R. Peltier, Department of Physics, University of Toronto, Toronto, Ontario, Canada M5S 1A7.

(Received February 28, 1984;
revised July 10, 1984;
accepted July 26, 1984.)